International Journal of Engineering Trends and Technology
ISSN: 2231–5381 / https://doi.org/10.14445/22315381/IJETT-V73I7P127

Volume 73 Issue 7, 339-356, July 2025

Original Article

COVID-19 Detection from Chest X-rays Using Pre-Trained Models and Compact Convolutional Transformers with Grad-CAM Visualization

Revathi A[1], Balaji Savadam[2]

[1,2]*Department of Computer Science and Engineering, Koneru Lakshmaiah Education Foundation, Hyderabad, Telangana, India.*
[1]*Department of Information Technology, VNR Vignana Jyothi Institute of Engineering and Technology, Hyderabad, Telangana, India.*

[1]*Corresponding Author : revathiannam@gmail.com*

Received: 27 January 2025 Revised: 01 July 2025 Accepted: 10 July 2025 Published: 30 July 2025

Abstract - *For the early and accurate detection of COVID-19, which is necessary for timely diagnosis and treatment, Chest X-Ray (CXR) imaging is crucial. Developing automated and reliable detection techniques is crucial because traditional diagnostic techniques, such as real-time Reverse Transcription-Polymerase Chain Reaction (RT-PCR), are time-consuming and prone to false negative results. This paper presents a compact and efficient Deep Learning (DL) system that uses pre-trained models and compact convolutional transformers to enhance feature extraction. The proposed model, TCovNet, uses an EfficientNet-B4 backbone and Gradient-weighted Class Activation Mapping (Grad-CAM) to generate comprehensible visual explanations for observed abnormalities. Additionally, contrast-limited adaptive histogram equalization CLAHE improves image clarity and model performance. The method was tested using balanced and imbalanced data distributions using publicly accessible COVID-19 CXR datasets. Experimental results demonstrate that TCovNet outperforms the current state-of-the-art techniques, with a classification accuracy of 98.5%. The use of Grad-CAM improves transparency and interpretability, making the model appropriate for clinical decision assistance. This study emphasizes the productivity of transformer-based architectures in medical imaging, besides the implication of explainability in DL-based COVID-19 diagnostic tools.*

Keywords - *Grad-CAM, X-ray, Convolutional Neural Networks (CNN), CLAHE, Edge computing, Deep Learning, Visualization.*

1. Introduction

The coronavirus disease was identified in Wuhan, China, before the end of 2019. According to current theory, it began in animals, quickly spread around the world, and was possibly subsequently conveyed by a host. After first being declared a global health emergency in January 2020, the World Health Organization (WHO) declared COVID-19 a pandemic in March 2020 [1]. The great majority of coronaviruses infect animals; however, some can infect humans. SARS-CoV-2, a coronavirus transmitted from bats to humans, poses a hazard to global health [2]. According to research, SARS-CoV-2 can live for a few hours or days on a variety of surfaces [3]. Many victims were infected by a novel coronavirus type termed Delta, which has more dangerous consequences and a short incubation period [4]. Direct contact, such as touching hands with an infected individual, and airborne transmission are the two main ways SARS-CoV-2 is transmitted. The virus replicates once it enters the respiratory system and destroys lung cells. COVID-19 is exciting to identify and treat due to its Ribonucleic Acid (RNA) changes. Coughing, fever, headache, dyspnea, confusion, and muscle pains are common signs of SARS-CoV-2 [5]. Serious outcomes, including death, are more likely to occur in those with weakened immune systems. Globally, COVID-19 has impacted nations and claimed a considerable number of lives [6]. Clinicians and experts in infectious diseases are working to create efficient treatments worldwide.

The most accurate method for detecting coronavirus disease and one that can help with early detection is the real-time Reverse Transcription-Polymerase Chain Reaction (RT-PCR) test, according to the WHO. For medical practitioners, RT-PCR testing can be hazardous and time-consuming [7]. To identify COVID-19 early, medical imaging techniques such as Computed Tomography (CT) scans, ultrasounds, and X-rays are frequently used. When combined with RT-PCR testing, these imaging methods assist doctors in making accurate diagnoses [8]. X-rays were one of the earliest imaging modalities utilized to determine COVID-19 due to their inexpensive cost and minimal radioactivity exposure.

Nevertheless, it is challenging to determine COVID-19 with X-rays [9]. White areas on the images that are loaded with pus and water must be recognized by radiologists; these areas are frequently faint and challenging to spot. Because diseases like pulmonary tuberculosis can exhibit symptoms that are similar to those of COVID-19, misdiagnosis is possible. The X-ray technology is therefore linked to a high rate of inaccuracy. Compared to X-rays, CT scans offer higher contrast and are more successful in identifying COVID-19. CT scans of SARS-CoV-2 patients show substantial consolidation, interstitial inflammation, and damage to the lung parenchyma [10]. However, analyzing COVID-19 with CT requires evaluating numerous slices for each patient, which can be time-intensive.

Specialists aim to exclude slices without critical information to streamline the process. In this regard, diagnostic imaging in conjunction with Artificial Intelligence (AI) has shown greater efficacy, especially when evaluating vital organs like the brain, heart, and lungs. This has prompted researchers to concentrate on creating AI-based techniques that will allow for faster, more affordable, and at-home COVID-19 identification, thus preventing the disease's spread [11]. Faster and more effective AI solutions are crucial since medical imaging datasets are scarce. CXR is desired above CT scans because of their lower radiation exposure, lower cost, and easier accessibility, even though CT scans are commonly used to assess COVID-19 [12]. This work emphasizes the procedure of CXR for COVID-19 finding in addition to examining the application of DL in visualization tasks such as image identification and classification.

DL has been gaining prominence as a solution for image classification challenges due to its improved results in illness identification [13]. In medical imaging, DL models have delivered robust and efficient outcomes for computer-aided diagnosis by extracting features that enhance classification accuracy. Using DL, researchers have created several designs for COVID-19 diagnosis. Others have modified pre-existing Convolutional Neural Network (CNN) models or created new ones. Coronet, coronavirus diagnosis-Net, and Xception with depthwise segmented convolution are a few examples that try to increase the efficacy of COVID-19 finding tasks. Others have employed Transfer Learning (TL) to diagnose using pre-trained models as feature weights. TL with CNN, deep CNN, MobileNet, and COVID-GAN are notable examples [14].

Numerous methods have been devised to automate the identification of COVID-19; at this point, these systems still encounter many challenges. Poor performance resulting from certain models' incapacity to efficiently extract features from input images is a major problem. Any AI-powered DL model must include feature extraction as a critical step, but limited and unbalanced datasets may restrict the creation of deep features and reduce diagnostic efficiency [15]. To address these issues, the experts have looked into using ensemble models. Whether pre-trained or created from scratch, these models combine two or more independent models to improve feature extraction and generalization. While ensemble models often outperform single models, there remains considerable room for improvement in their outcomes.

One of the most advanced techniques for visual tasks is the attention mechanism [16]. By transmitting relative weights to input attributes based on their significance to a certain job, this approach helps to highlight vital qualities while lessening the influence of less significant ones. In ensemble modeling, convolutional layers extract visual information from the input images. While removing unnecessary features, these layers seek to preserve important ones. Critical characteristics are occasionally disregarded, though, which results in insufficient feature extraction and possible COVID-19 misclassification [17, 18].

The automated classification of lung infections from CXR images has significantly improved in recent years due to advancements in deep learning. However, there are still several problems with the existing methods. Most conventional approaches either do not generalize well across a range of patient populations or employ small datasets, which results in biased models. Numerous deep CNNs utilized in earlier studies are also computationally intensive and prone to overfitting, especially when used on small or unbalanced datasets. Furthermore, clinicians find it difficult to trust the predictions made by these models because they are typically not interpretable.

To address these limitations, the suggested model, TCovNet, combines the potent EfficientNet-B4 backbone with Grad-CAM to highlight significant regions influencing model decisions, thereby introducing an innovative and interpretable Deep Learning (DL) structure for coronavirus disease detection by CXR images. CLAHE, which is incorporated into TCovNet in contrast to standard models, improves local contrast and fine-grained lung textures, hence increasing the accuracy of feature extraction and classification. The model shows strong performance and generalizability after thorough testing on publically accessible CXR datasets with both balanced and unbalanced data distributions. By combining explainable AI, efficient architecture, and improved preprocessing, TCovNet substantially contributes to accurate and transparent Coronavirus diagnosis. This approach facilitates a deeper sympathy for the logic of the model, which makes it easier to apply in clinical settings for accurate Coronavirus diagnosis. An overview of the study's primary contributions is provided below:

- A lightweight convolutional transformer-based DL system was introduced, incorporating Grad-Cam-enhanced CLAHE visualization for fast and precise COVID-19 prediction using CXR images.

- EfficientNet-B4, the backbone network, was developed using a fusion concatenated technique to offer robust and superior deep features. The convolutional ViT overcomes the drawbacks of the CNN layer's maximum pooling, which frequently ignores important spatial information about picture components, by using positional anchoring and patching techniques. Additionally, by emphasizing the areas of the image that were most pertinent to the categorization results, Grad-Cam was used to understand model predictions.
- Experimental evaluation of the recommended framework's performance was conducted in several dataset classification tasks, such as binary and multi-class prediction tasks. Using Grad-Cam to create visual saliency maps, the study also showed that the framework can accurately and simultaneously forecast several diseases.

The following is the plan for this study: Relevant research is the main topic of Section 2. While Section 4 outlines the investigational findings and assessments, Section 3 thoroughly explains the recommended methodologies. The findings are concluded in Section 5.

2. Literature Survey

Predicting COVID-19 from CXR pictures has become a crucial research topic, utilizing AI and DL to support quick, non-invasive diagnosis. Ground-glass opacities and consolidations are two important lung abnormalities associated with COVID-19 that can be seen with CXR, which is widely available and reasonably priced. Due to the time and resource constraints of conventional diagnostic techniques like RT-PCR and DL models in particular, CNNs have been used to automate the identification of these patterns. Numerous studies have shown that AI has the potential to improve identification speed and accuracy, providing vital assistance in clinical decision-making throughout the epidemic. However, ongoing challenges, including limited labeled data and variability in X-ray quality across populations, indicate the need for further research and model refinement. The existing papers are surveyed in this section.

Ukwuoma et al. [19] proposed deep feature concatenation and a multi-head self-management network as elements of an end-to-end DL architecture. The feature concatenation technique optimizes previously learned backbone models, such as DenseNet, InceptionV3, and Visual Geometry Group-16 (VGG-16). The suggested model performed well on the multi-class and binary classification tasks, achieving 96.35% and 98.65% total precision and 92.65% and 98.65% F1 scores, respectively. However, DL models are still susceptible to hostile attacks, which highlights the need for more robust security measures. Nayak et al. [20] presented a novel lightweight DL technique constructed on CXR for multi-class classification. Three convolutions make up the suggested CNN architecture for batches of normalization: a fully connected layer, a Global Mean Pooling (GMP) layer, and ReLU blocks with learnable parameters. The model accomplished a satisfactory overall accuracy of 98.30% compared to State-of-the-Art (SOTA) methods and pre-trained Transfer Learning (TL) models. However, due to variations in the number of channels and input image sizes, the tiny dataset used to test the proposed method faced challenges. These discrepancies impair the model's durability.

Houssein et al. [21] recommended a Hybrid Quantum-Classical CNN (HQ-CNN) model using random quantum circuits for coronavirus identification using CXR images. The model's accuracy and recall on multi-class datasets were 88.20% and 88.60%, respectively. However, to conform to minimal quantum technology, the HQ-CNN design is constrained by its dependence on a small number of layers. Thus, the method's shortcomings are brought to light by its difficulties with big datasets and classification with multiple classes of jobs.

Meem et al. [22] demonstrated the procedure of CNN, DL, and Machine Learning (ML) to distinguish between coronavirus patients and healthy individuals using CXR images. The model is constructed using several DL features, including Maxpooling 2d, Dense Net, Dropout, and the 2D Convolutional Layer (Conv2D). The proposed technique achieved 98.33% validation accuracy and 96.43% classification accuracy after training and testing on X-ray images. However, epoch 1 validation accuracy heights begin to somewhat decrease after epoch 7.

Ukwuoma et al. [23] established a trustworthy DL method for correctly identifying lung conditions from CXR pictures. The recommended method allows for a comprehensive analysis of CXR images by using an ensemble strategy to extract richer features and then overall second-order pooling to collect even more detailed global characteristics. The accuracy of the model was 98.00% on the COVID-19 dataset and 97.80% on the COVID-CXR-15k dataset. However, this study did not look at how to improve image qualities or whether lung sickness was reasonable, mild, or severe.

Rahhal et al. [24] recommended a DL-based COVID-19 ultrasound image identification technique. The method combines TL with an EfficientNet model previously trained on the ImageNet dataset to classify ultrasound images of probable patients. A gated multilayer perceptron (gMLP) and a ViT were used to compare the efficacy of EfficientNet-B2. The EfficientNet-B2 model achieved precision, recall, and F1 scores of 95.85%, 99.87%, and 97.43% for COVID-19 classification, respectively. With TL, EfficientNet-B2 achieved an accuracy of 96.75%, overtaking gMLP (93.13%) and ViT (92.83%). However, learning a lot of parameters is necessary for the suggested EfficientNet-B2 model.

Albahli et al. [25] proposed a technique that uses CT scans and X-ray pictures to identify the affected areas in addition to detecting COVID-19. The model leveraged pre-trained classification architectures like VGG-16, VGG-19, and ResNet50 with very slight adjustments. Using CT scan images, the ResNet50 model showed a maximum validation accuracy of 87.13% and a training accuracy of 87.49%. The maximum validation and training accuracy of the VGG-16 model for X-ray images were 97.37% and 95.60%, respectively. However, when the VGG-19 model was used, the validation accuracy decreased to 86.37%.

Srinivas et al. [26] introduced "Inception V3 with VGG16", a novel hybrid technique for COVID-19 prediction that uses CXR. This model combines two DL models, IV3-VGG. The hybrid scheme comprises of two parts: pre-processing and IV3-VGG. The investigational outcomes indicate that the IV3-VGG model overtakes the five most popular DL models currently in use with an accuracy of 98.00%. It is necessary to extend the proposed model to accommodate huge X-ray datasets.

In their work, Umer et al. examined how a CNN collects COVID-19 prediction data from CXR images [27]. Applied the categorization procedure to classes 2, 3, and 4. CXR images from COVID-19, normal, viral pneumonia, and bacterial pneumonia are included in the four-class scenario. The suggested approach obtained an AUC value of 59.48%, a sensitivity of 98.99%, and a specificity of 92.19% when tested and trained on the four-class dataset. The model must be expanded to handle more X-ray datasets to produce better results.

The CXR6, a lightweight CNN designed for automatic pneumonia detection, was introduced by Nahiduzzaman et al. [28]. The CXR6 model was trained and maintained for binary classification, distinguishing between common and pneumonia cases, to demonstrate its generalizability. With a recall of 98.00% and an accuracy of 97.95%, the pre-trained CXR6 model fared better than SOTA models for binary classification. Even if the model did well on the combined dataset, it might not do as well on other datasets.

Hybrid CNN (HDCNN), a new technique for COVID-19 detection using CXR that combines the design of CNN with Recurrent Neural Networks (RNN), was presented by Kumar et al. [29]. The images that produce judgments are shown by HDCNN employing a TL technique known as slope-weighted activating class planning (Grad-Cams). Consequently, HDCNN obtained a 97.00% F1 score, 97.35% precision, 97.10% recall, and 98.23% accuracy. The performance may still be better, though. Arivoli et al. [30] suggested a DL methodology that processes CXR images to detect COVID-19. A CNN is constructed using Keras, and a user-friendly, controllable front-end interface is included. The recommended method's classification accuracy was 99.00%. Using CoviExpert on any device, doctors can quickly identify which patients have COVID-19. Because a few X-ray samples were used in the investigation, deployment was delayed.

The useful work done thus far has a common drawback: it has mostly been applied to datasets that were too small because of a lack of data. This increases the chance of errors in real-world applications, even with excellent performance. In other cases, the model had a sufficiently large dataset, but its accuracy and efficiency were not properly matched. After a thorough analysis of these variables, a well-built architecture intended to provide outstanding and effective performance on a properly selected and processed dataset has been developed. Achieving exceptional results, especially in 3-class classification, is the main driving force behind the proposal of a novel architecture. The following sections provide an overview of the proposed architecture's specifics.

3. Materials and Methods

The suggested model pipeline uses CXR images to identify coronavirus. The input CXR image dataset is pre-processed, utilising data augmentation and CLAHE to enhance image quality and diversity. The EfficientNet-B4 model, the main feature extractor and classifier, receives the pre-processed images. The areas of the image that affected the prototype's classification of the image as either normal, viral pneumonia or COVID-19 are shown using the Grad-CAM technique. The suggested architecture is shown in Figure 1.

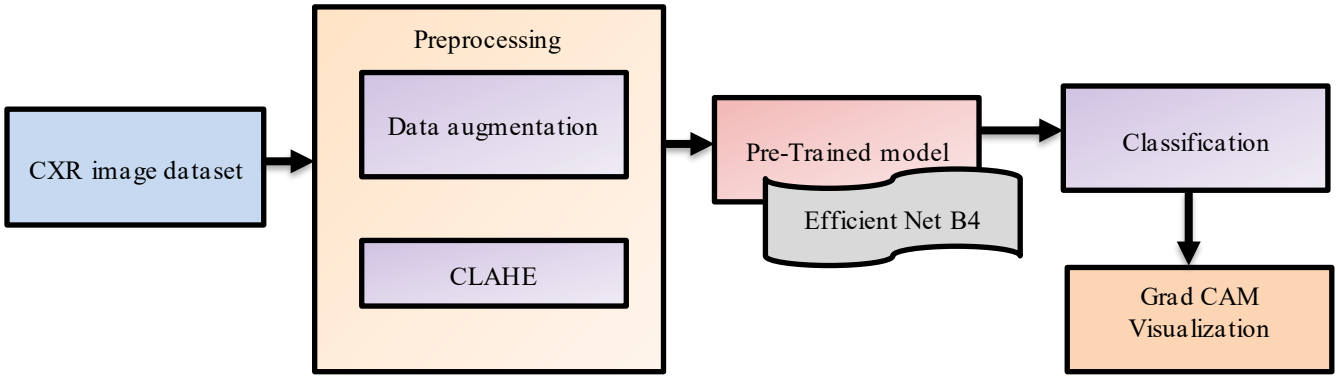

Fig. 1 Block schematic for the suggested approach

3.1. Image Dataset

In this work, CXR images were used to diagnose. The dataset comprised three forms of pneumonia: normal, viral, and COVID-19. The "COVID-19 Radiography Database," which is publicly available on platforms like Kaggle, is where the images were taken. 70% of the dataset was reserved for training and validation, while 30% was reserved for testing. In the training-validation set, 70% was allocated to training and 30% to validation. Table 1 provides a description of the dataset distribution, while Figures 2 through 4 display representative samples.

Table 1. Dataset description

Class	Image count	Size
COVID-19	800	224*224
Normal	2500	224*224
Viral	5000	224*224
Total	9300	224*224

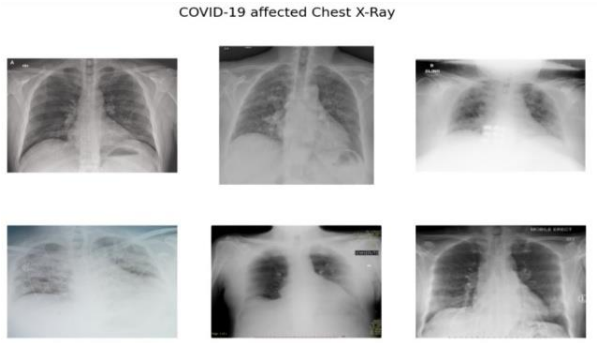

Fig. 2 CXR samples analyzed with the dataset

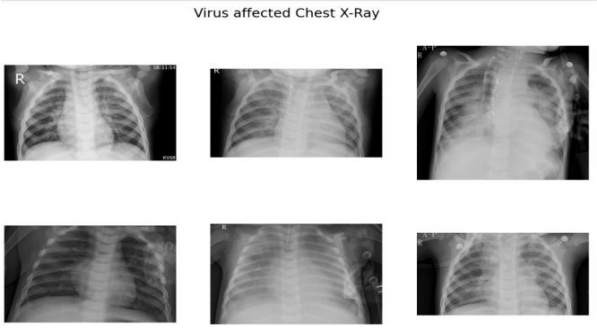

Fig. 3 The CXR viral image samples

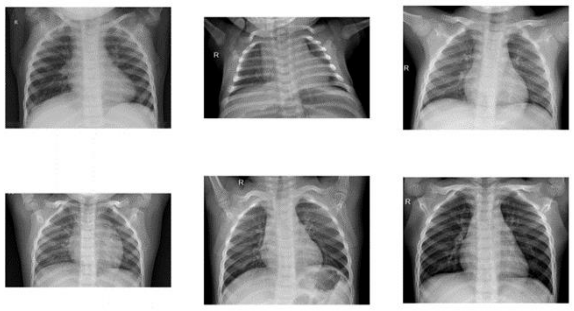

Fig. 4 The CXR normal image samples

3.2. Data Pre-Processing

Data augmentation and CLAHE were two preprocessing techniques to enhance model generalization and image quality.

3.2.1. Augmenting Data

Data augmentation is the process of using modified versions of pre-existing photographs to artificially escalate the size of the training set. This strategy affords an extra diverse array of training data, improving the models' longevity and effectiveness. The following augmentations are used:

Flips (Horizontal & Vertical): Randomly selected images from the original training set are flipped both vertically and horizontally. Additionally, the flipped photographs are simultaneously saved in two separate folders named "Horizontal Flips" and "Vertical Flips," respectively.

Rotation: At angles between 20 and 90 degrees, randomly chosen photos from the initial training set are rotated. After that, the rotated photos are saved independently in a folder called "Rotation."

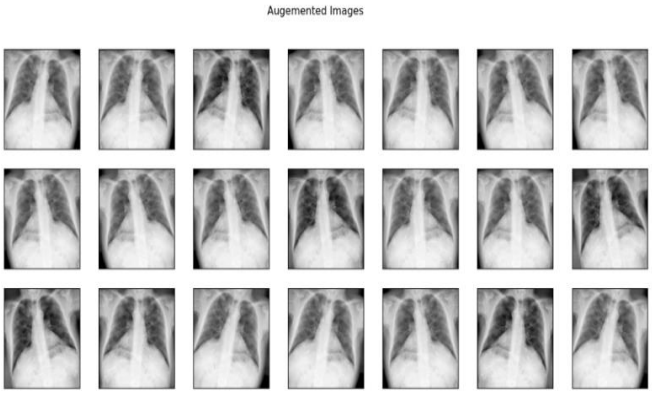

Fig. 5 Enhancement of images by flipping them both vertically and horizontally with a rotation range

3.2.2. CLAHE

CLAHE is a sophisticated Histogram Equalization (HE) technique that enhances local contrast while reducing noise. CLAHE separates a picture into contextual tiles, applies adaptive equalization inside each tile, clips the histogram at a predetermined threshold, and then evenly redistributes surplus contrast, in contrast to global HE, which has the potential to oversaturate bright areas. Its application significantly enhanced the visibility of lesion boundaries and fine lung textures in chest X-ray images. Average feature-map activations in early convolutional layers increased by 2% to 3% compared to standard HE, indicating richer feature extraction. As a result, the model showed a 1.5% improvement in COVID-19 recall, as it could more effectively detect faint opacities typical of early-stage infections. Figure 6(a) shows the original image, and Figure 6(b) shows the CLAHE-enhanced image.

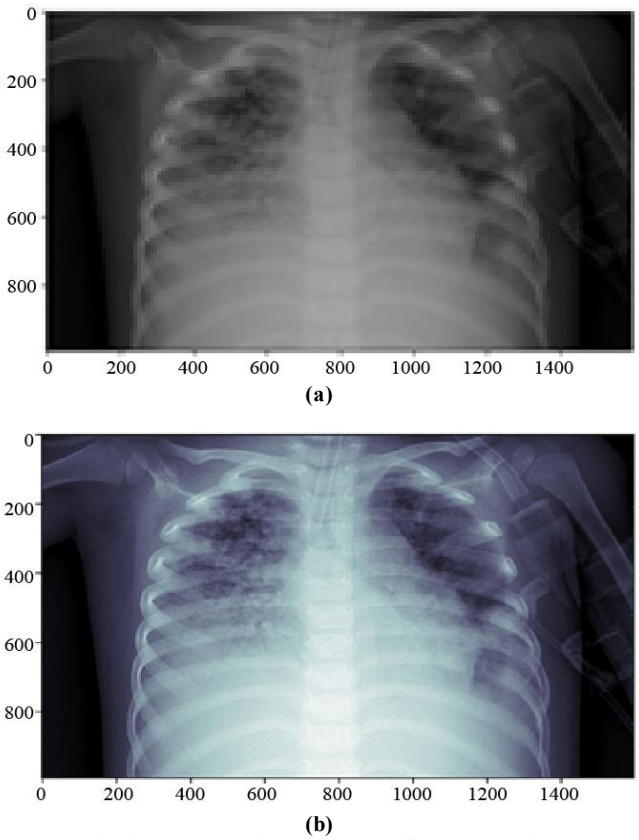

Fig. 6(a) Regular image, and (b) CLAHE applied.

3.3. Pre-Trained Model for Classifying Images

This study mainly aims to categorize COVID-19 images from CT and X-ray to identify the problematic area. Pre-trained representations were used and improved in order to achieve this.

Pre-trained representations are modified to fit another dataset after being trained on the first one. Requiring fewer training epochs is an advantage of using pre-trained representations.

3.3.1. EfficientNet-B4 Model

The TCovNet- EfficientNet-B4 model is a specific architecture within the EfficientNet family of CNN models, proposed [42]. It is well known for striking an outstanding balance between computing performance, accuracy, and model size. The base Efficient Net model, EfficientNet-B0, starts with a relatively small network and scales it up to obtain larger versions such as B1, B2... B7.

Efficient Net models use complex scaling to achieve equilibrium depth, width, and resolution. EfficientNet-B4 is especially well-suited for applications with constrained computational resources because of its scaling method, which enables it to achieve higher performance on image classification tasks while preserving computational efficiency. Table 2 displays the EfficientNet-B4 network parameters, and Figure 7 shows the network structure.

Table 2. Title of the table

Stage	Operator	Input	Output Channels	Stride
1	Conv=3 × 3	380 × 380	45	1
2	MBConv1,k=3 × 3	190 × 190	22	2
3	MBConv6,k=3 × 3	190 × 190	34	4
4	MBConv6,k=5 × 5	95 × 95	56	4
5	MBConv6,k=3 × 3	95 × 95	112	5
6	MBConv6,k=5 × 5	48 × 48	157	5
7	MBConv6,k=5 × 5	48 × 48	269	7
8	MBConv6,k=3 × 3	24 × 24	448	2
9	Pooling & FC	24 × 24	1792	1

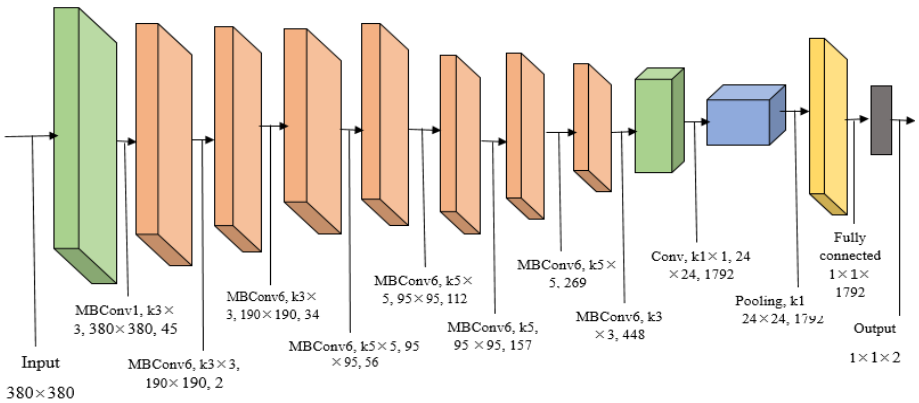

Fig. 7 Structure of the EfficientNet-B4 model

3.4. GRAD CAM Architecture

Following the classification phase, the research aims to identify the regions of CXR images affected by COVID-19. Heat maps are created for each layer of the neural network using the Grad-CAM localization technique, which gives a broad overview of DL models. This approach aids in both identifying and predicting the problem at hand and helps us understand how the models make decisions. A basic Grad-CAM approach notion is shown in Figure 8. Grad-CAM initially determines the expected class using a pre-trained model. The last convolutional layers of the network are then traced by iterating over the architecture in reverse order. The gradient model was utilized in this work to highlight the regions of the input image that remain most crucial for classification, resulting in heat maps that show the COVID-19-affected areas.

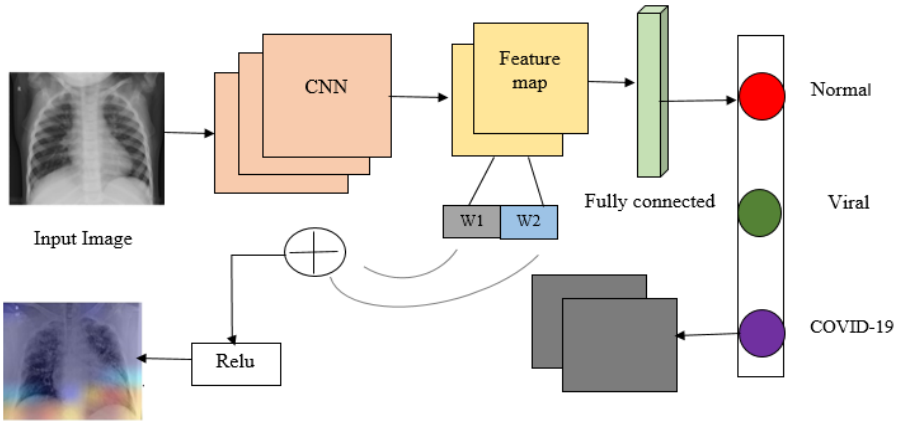

Fig. 8 GRADCAM architecture

Training model: The CNN model was trained using task-relevant datasets, like lung image classification for respiratory illnesses. Take the feature out of the trained model's selected convolutional layers.

Feature extraction: The trained model's selected convolutional layers can be used to extract feature maps. Let us denote these feature maps as $A^{(k)}$ representing the index of the layer as presented in (1).

$$L^{(c)} = \sum_i \alpha_i^c A_i^{(k)} \quad (1)$$

Where $A_i^{(k)}$ is the i^{th} layer's feature map k, and α_i^c is the weight associated with it.

Gradient calculation: About the feature map, the gradients of the object class score should be found using Equation (2).

$$\frac{\partial y^c}{\partial A_i^{(k)}} \quad (2)$$

Where y^c is the target class's score.

Global Average Pooling: Take the GAP of the gradients obtained in the previous step as per Equation (3).

$$\alpha_i^c = \frac{1}{z}\sum_j \sum_k \frac{\partial y^c}{\partial A_i^{(k)}} \quad (3)$$

Where z is the total number of elements in the gradient.

Combined weights: Grad-CAM was applied to the last MBConv block of EfficientNet-B4 by first calculating each target-class score's gradient in relation to the feature map locations. Channel-wise weights (α_i^c) were obtained via global average pooling of these gradients, then linearly combined with their corresponding feature maps and passed through a ReLU to produce the class-specific heatmap:

$$L_{Grad-cam}^{C} = Re\ L\ U\left(\sum_k \alpha_i^c A_i^{(k)}\right) \quad (4)$$

$\sum_k \alpha_i^c A_i^{(k)}$ symbolizes the feature maps' weighted combination according to their significance scores for the class C. The resulting heatmaps were overlaid on the CLAHE-enhanced CXRs using a semi-transparent jet colormap.

Qualitatively, the maps consistently localized to peripheral bilateral opacities in COVID-19 cases and consolidation patterns in viral pneumonia, demonstrating that CLAHE not only improved classification accuracy but also sharpened the spatial precision of saliency visualizations.

3.5. Statistical Significance

The data was confirmed using several overfitting correction techniques. To improve generalization and reduce overfitting during training, dropout layers, early stopping, and data intensification techniques with overturning and rotation were employed.

Five-fold cross-validation was used to further assess the model's endurance, and it performed consistently across all

folds. Additionally, a baseline CNN model and the suggested EfficientNet-B4 model were connected using a paired t-test. According to the findings, the observed improvements in accuracy and F1-score were statistically significant and not the result of chance, with a p-value less than 0.05.

4. Results and Discussion

This division compares and contrasts the effectiveness of COVID-19 prediction from CXR employing a pre-trained model, compact convolutional transformers, and Grad-Cam-Based visualization to existing techniques.

Another pre-trained model, ResNet50 [31], VGG16, VGG19 [32], Xception [33], and InceptionV3 [34], was used to evaluate the efficacy of the efficient net model B4.

4.1. Dataset Description

The learning used the publicly available COVID-19 Radiography Database on Kaggle, which consists of three classes of clearly labeled CXR images: COVID-19, Viral Pneumonia, and Normal. Because of its extensive use in prior research, reliable annotations, and equitable representation of the many forms of pneumonia that allow for comparison analysis, this dataset was chosen. A total of 800 COVID-19, 2500 Normal, and 5000 Viral Pneumonia images were used; each image was resized to 224 by 224 pixels to encounter the input requests of the pre-trained model. The dataset was divided into 70% for training and 30% for evaluation to allow for reliable model design and tweaking. Following that, subsets of the training set were allocated into training and validation subsets in a 70:30 ratio. The four distinct datasets utilized to train the four models are displayed in Table 3.

Table 3. Dataset arranged for classification

Models used for classifications			Training	Testing	Validation
X-ray	Original	COVID-19	700	300	100
		Normal	4000	1000	750
		Viral	2500	800	400
	Balanced	COVID-19	700	300	150
		Normal	1500	300	125
		Viral	1700	300	135

4.2. Performance Metrics

The experiment was conducted using the following five criteria to examine the performance metrics. Table 4 summarizes these performance metrics and the calculations that go along with them.

Table 4. Performance metrics

Performance metrics	Formula
Accuracy	$\frac{(\mathrm{TNi}+\mathrm{TPi})}{(\mathrm{TNi}+\mathrm{TPi}+\mathrm{FNi}+\mathrm{FPi})}$
Precision	$\frac{TPi}{(TPi+FPi)}$
Recall	$\frac{TPi}{(TPi+FPi)}$
F1-score	$Fi=\frac{2PRi}{Pi+Ri}$
Specificity	$\frac{TNi}{TNi+Fpi}$

The model's behavior and the outcomes it produced on chest X-ray images of both healthy and sick people are clearly described by the terminology employed. A "positive" prognosis indicates "COVID-19," whereas a "negative" one indicates "normal."

Figure 9 displays the classification accuracy of several DL models for COVID-19 detection by CXR images. The suggested method outperformed all other models examined, with a maximum accuracy of 96.5%. Xception and Inception V3 have respective accuracy ratings of 87 and 88. Specifically, VGG19, ResNet50, and VGG16 had lower accuracy scores (84%, 85%, and 84%, respectively). These results demonstrate that EfficientNet-B4 has the highest reliable accuracy among all the models analyzed.

Figure 10 shows the precision scores of several DL models for coronavirus diagnosis using CXR images. The suggested model has a lower false positive rate and a higher precision rate (95%) when it comes to detecting positive scenarios. The precision ratings for Xception and InceptionV3 are 86% and 87%, respectively. VGG19, ResNet50, and VGG16 have lower precision scores (84%, 83%, and 82%, respectively). These findings demonstrate that EfficientNet-B4's accuracy continuously outperforms the other models.

Figure 11 displays the recall performance of many DL models for detecting coronavirus from CXR images. With the highest recall score of 96%, the suggested model is significantly capable of correctly identifying actual positive events and removing false negatives. Xception, InceptionV3, and ResNet50 achieved comparable recalls of 85%, 86%, and 84%, respectively. Recall ratings were lower for VGG19 and VGG16 (83% and 81%, respectively). These results show that EfficientNet-B4 has the highest recall, making it perfect for critical coronavirus detection tasks where reducing the percentage of missing real events is essential.

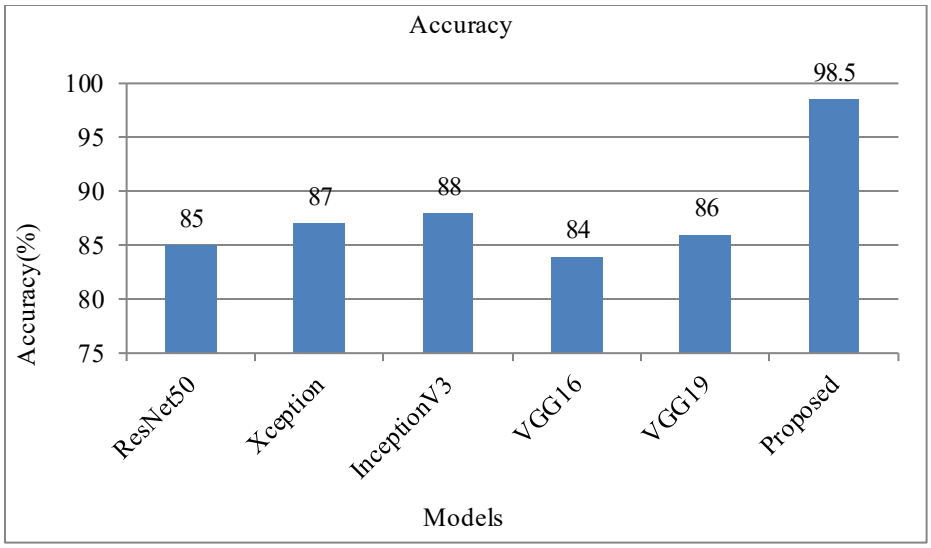

Fig. 9 Comparison of the performance of accuracy for classification using CXR images

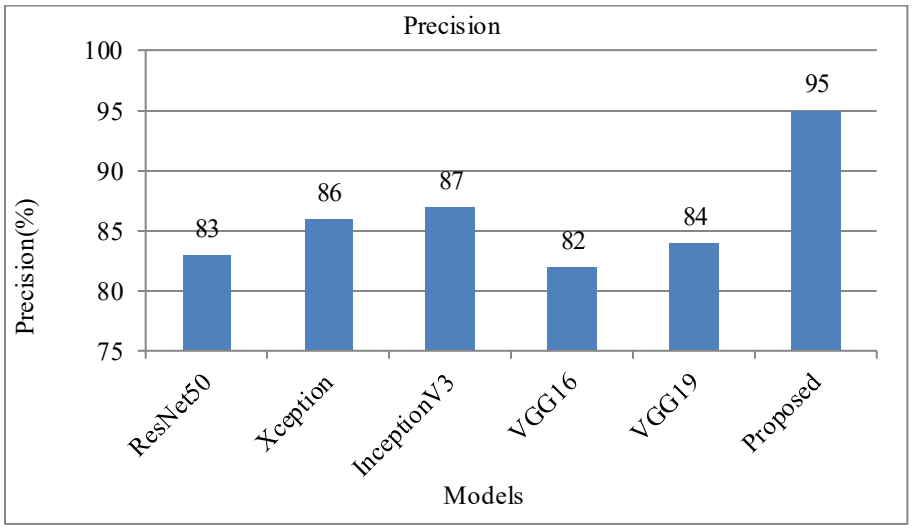

Fig. 10 Comparison of precision performance

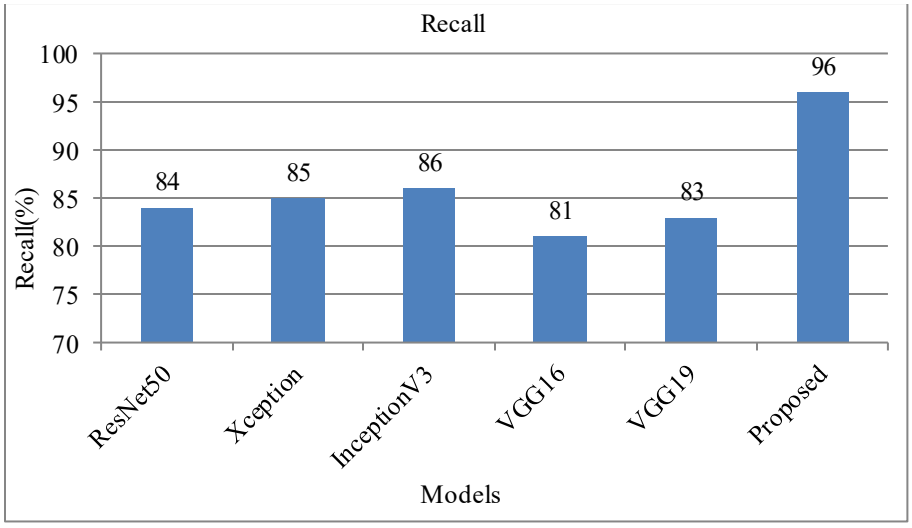

Fig. 11 Comparison of recall performance

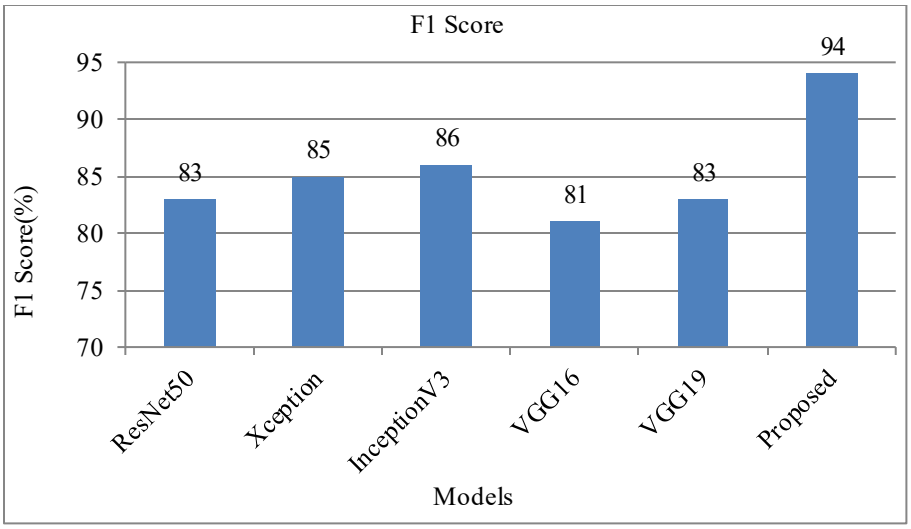

Fig. 12 Comparison of the performance of the F1-score

Figure 12 displays the F1 score performance for various models used to categorize COVID-19 from CXR images. The suggested method exhibits improved whole classification performance, effectively balancing recall and precision, with the greatest F1 score of 94%. ResNet50, Xception, and InceptionV3 have respective F1 scores of 83%, 85%, and 86%. VGG19 has the highest score at 83%, while VGG16 has the lowest at 81%. These results demonstrate that EfficientNet-B4 is the most reliable model among those evaluated, producing predictions that are both accurate and consistent.

4.3. Classification Process

This study's primary goal is to categorize COVID-19 X-rays and identify the affected regions in images. Classification was done using pre-trained models, which were then improved to detect coronavirus cases more accurately and efficiently. The efficacy of the efficient net model B4 was compared with various pre-trained models, comprising Xception, InceptionV3, VGG16, VGG19, and ResNet50. Table 5 displays the accuracy and loss for training, testing, and validating models that were trained on these datasets. With a batch size of eight and a 90-degree image rotation, each model was trained across 30 training epochs. The findings show that across both datasets, ResNet50, Xception, InceptionV3, VGG16, and VGG19 continue to have consistently low accuracy. Even though the dataset was balanced or CLAHE, these models still performed poorly. Although TCovNet-EfficientNet-B4 showed relatively higher accuracy, it fell short compared to the literature's reported accuracy levels. Because EfficientNet-B4 uses compound scaling, a novel technique that consistently scales network dimensions. This means that EfficientNet-B4 can be scaled to larger networks more efficiently than traditional architectures.In comparison, ResNet, VGG, and other models scale each dimension independently, often leading to inefficiencies. EfficientNet B4's scaling allows it to extract better features from high-resolution medical images while maintaining computational efficiency. The total number of parameters used for experiments on image size is mentioned in Table 6.

Table 5. Parameters used for model experiments

Name of the Model	No. of Parameter	Image Resolution
ResNet50	21.1	224*224
Xception	22	299*299
InceptionV3	23	299*299
VGG16	138	224*224
VGG19	143	224*224
Efficient net-B4 (Proposed)	15.8	350*350

Table 6. Accuracy and loss attained by various models during training, testing, and justification on X-ray images

Samples	Models	Accuracy of Training	Accuracy of Testing	Loss of Training	Loss of Testing	Val-Acc	Val-Loss
BALANCED and CLAHE	ResNet50	0.72	0.60	0.10	1.81	0.70	1.10
	Xception	0.67	0.46	0.50	1.33	0.73	0.23
	InceptionV3	0.80	0.57	0.67	3.22	0.79	0.24
	VGG16	0.82	0.72	0.22	4.15	0.45	3.34
	VGG19	0.80	0.62	0.12	2.54	0.42	1.15
	Efficient net-B4	0.96	0.87	0.12	0.92	0.82	1.11

BALANCED	ResNet50	0.73	0.84	0.55	0.27	0.82	1.12
	Xception	0.70	0.37	0.72	2.30	0.76	0.61
	InceptionV3	0.56	0.42	0.89	0.79	0.43	0.89
	VGG16	0.80	0.84	0.23	3.23	0.23	2.23
	VGG19	0.70	0.72	0.22	1.24	0.17	1.23
	Efficient net-B4	0.94	0.91	0.17	0.68	0.81	0.43

EfficientNet-B4 achieved the highest accuracy for both CLAHE and BALANCED datasets among the X-ray images. CLAHE and BALANCED datasets yielded the highest accuracy for the EfficientNet-B4 model. When using EfficientNet-B4, Balancing and contrast enhancement are concurrently proving the better COVID-19 classification, reaching the accuracy of 0.9634. However, the existing models attained lower accuracy than the existing models. A balanced dataset ensures that all classes are equally represented, minimizing the risk of model bias toward the majority class. This leads to more reliable and generalizable predictions, which are especially important in medical contexts where an imbalanced dataset could cause the model to overlook minority cases. CLAHE enhances the local contrast of X-ray images, making subtle features (like lung opacities or early signs of infection) more prominent. EfficientNet B4, with its advanced feature extraction capabilities, benefits from this enhanced input, allowing it to identify better key patterns associated with COVID-19. Also, EfficientNet-B4 integrates Squeeze-and-Excitation (SE) blocks, which help the model emphasize the most significant features in an image, improving its ability to identify crucial regions affected by COVID-19 (such as lung opacities in CXR). These SE blocks dynamically recalibrate channel-wise feature responses, enhancing the detection of subtle and critical features, which are crucial in early coronavirus detection. However, VGG16 and VGG19, while deep, tend to overfit on small medical datasets due to their large number of parameters, and ResNet50 might not be as efficient in extracting fine-grained details in medical images. Therefore, it will provide lower efficiency while applying a balanced CLAHE image or only a balanced image. The EfficientNet-B4 visualization model results are shown in Figure 13.

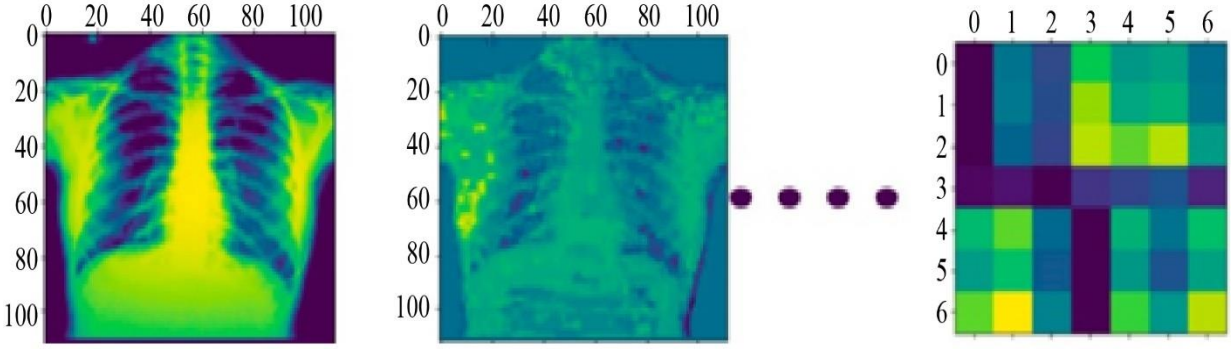

Fig. 13 EfficientNet-B4 model heat map visualization

4.4. Localization

To determine the areas impacted by the disease, each trained model is ultimately put via the Grad-Cam.

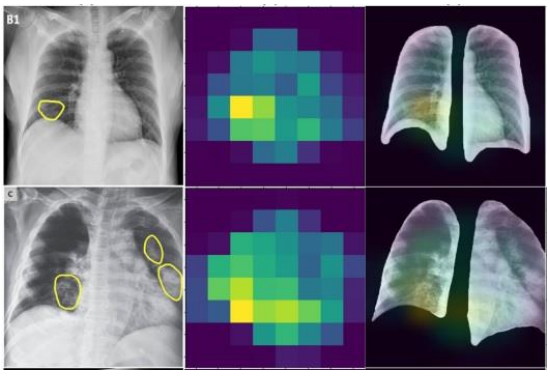

Fig. 14 Extracted heat map using the GRADCAM algorithm

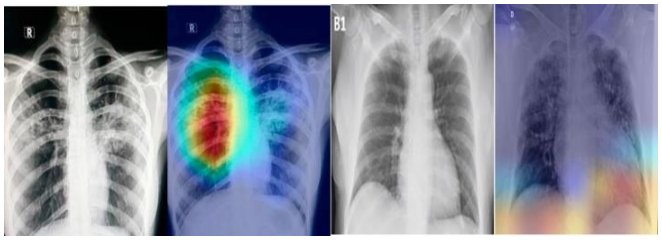

Fig. 15 Visualization of heat maps using the GRADCAM algorithm

The photos illustrate that the model developed on the initial data set correctly emphasized the affected area compared to the model built on upgraded images.

The localization becomes more accurate the higher the accuracy. The determination of the image also has a bearing on localization shown in Figures 14 and 15.

4.5. Results for Classification Obtained

The TL model performed an excellent classification of COVID, normal, and viral with promising results, as shown in Figure 16.

The production of a classification system is often assessed using a confusion matrix and a validation set of known true values, as shown in Figure 17. In this matrix, a forecast label instance is shown by each column, and an actual label occurrence is indicated by each row.

The diagonal values in the matrix represent how many test photos the model correctly predicted for each class. The confusion matrix displays the presentation of a COVID-19 classification model by classifying X-ray pictures as either normal or viral (non-COVID) X-rays. According to the matrix, the model correctly identified 131 normal X-rays, but incorrectly classified four as viral and one as COVID-19. It accurately identified 112 of the 116 COVID-19 X-rays; just one was mislabeled as normal, and two as viral. Finally, the model was able to correctly predict 106 out of 113 viral X-rays, with five cases being incorrectly labeled as normal and two cases being incorrectly identified as COVID-19. With few misclassifications across all categories, the model generally shows good accuracy, primarily in differentiating individual COVID-19 from other X-ray forms.

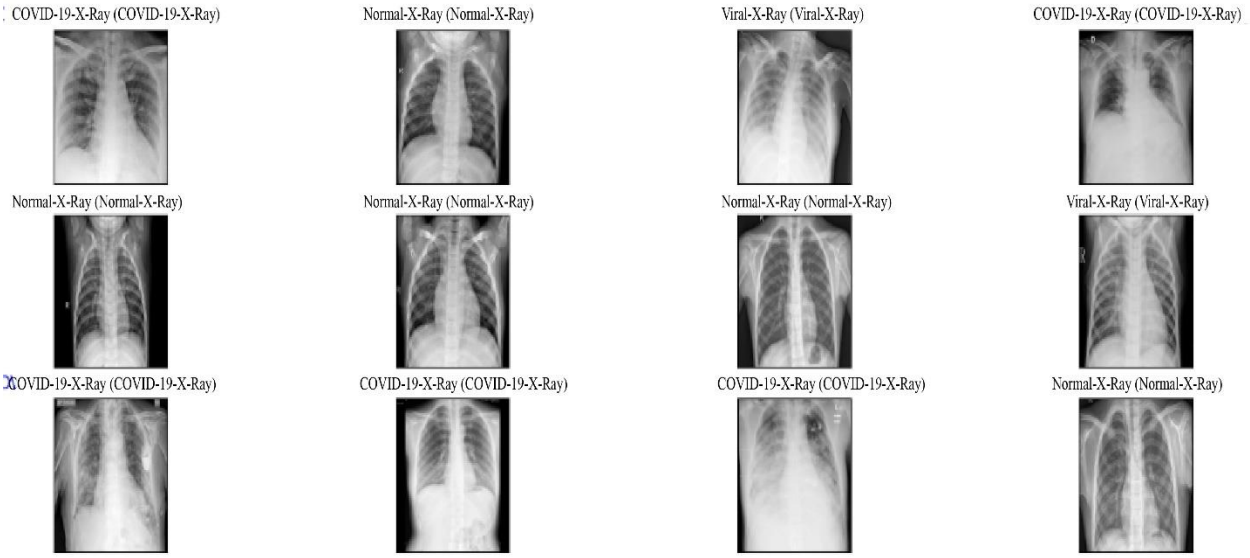

Fig. 16 The classification results obtained

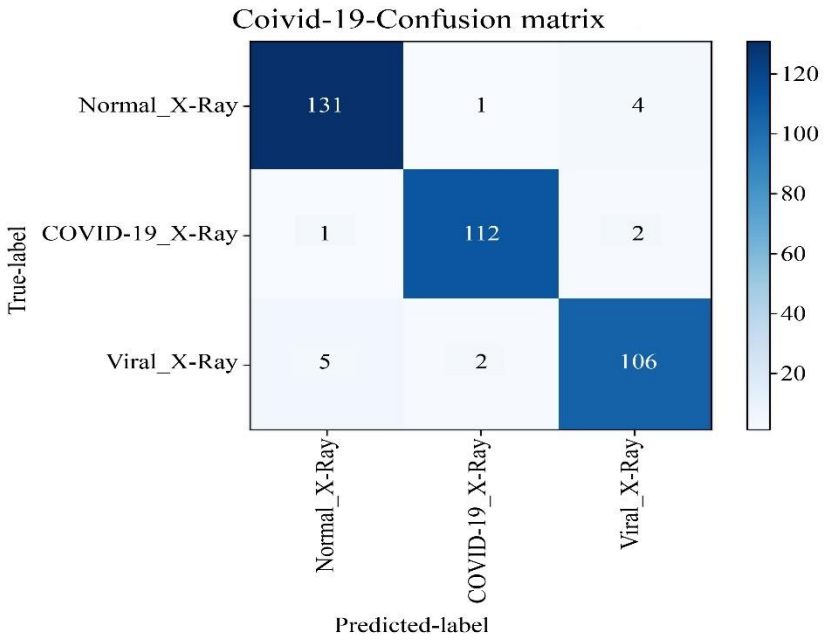

Fig. 17 The validation dataset's diagnostics confusion matrix

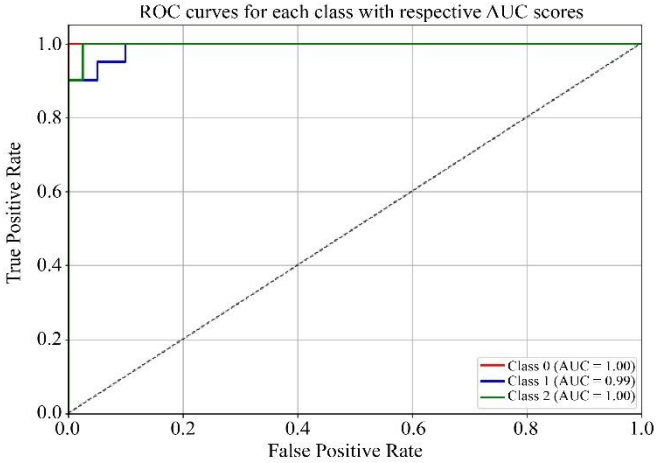

Fig. 18 The ROC curve under the AUC score

Figure 18 shows the ROC curve, which contrasts the rates of true positives and false positives at various threshold settings. This graph displays the classification model's performance at various thresholds as well as its capacity to distinguish between positive and negative categories.

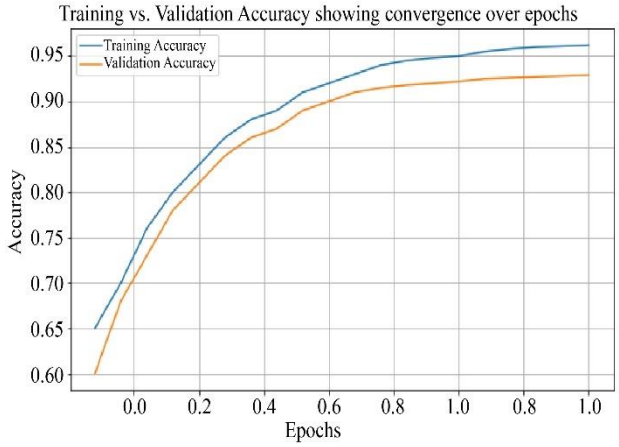

(a)

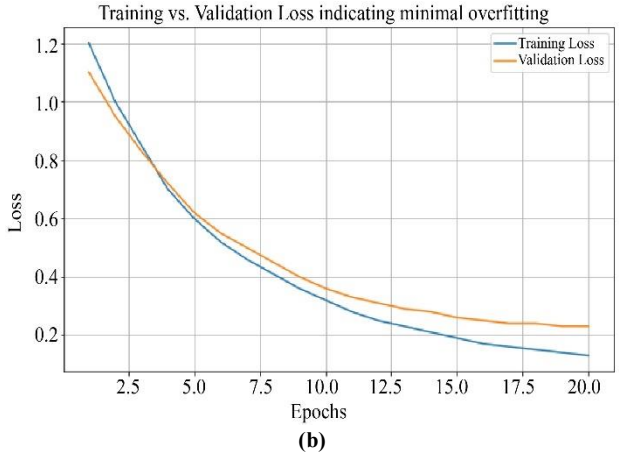

(b)

Fig. 19 Curves of training and validation for the suggested method, (a) training and validation accuracy, and (b) training and validation loss curve.

In the domain of medical diagnostics, a greater AUC means that the model can more accurately identify both favorable and unfavorable situations. ROC curves for normal, COVID-19, and the three classes (0, 1, and 2). The curves in the upper-left corner for each class show that the model has good predictive ability and high true positive rates and low false positive rates.

Figure 19(a) shows the convergence of the training and validation accuracy of the proposed model throughout 20 epochs. At the start of period 1, training accuracy is approximately 65% and validation accuracy is approximately 60%. Both metrics show a consistent upward trend as people improve with coaching. Epoch 10 shows effective learning and generalization with a training accuracy of over 92% and a validation accuracy of over 90%. The model continues to improve after epoch 10, reaching a peak training accuracy of roughly 96% and a settling validation accuracy of roughly 93% by epoch 20. A well-generalized model with less overfitting is indicated by the little difference between the two curves throughout the training phase.

Figure 19(b) displays the training and validation loss curves over 20 epochs, highlighting the model's modest overfitting and convergence. At epoch 1, the training loss begins at approximately 1.2, and the validation loss starts near 1.1. Both losses decrease consistently, with training loss falling below 0.6 and validation loss just above 0.6 by epoch 5. The decline continues smoothly, and by epoch 10, training loss is around 0.35, while validation loss is near 0.4. Toward the final epochs, training loss reaches approximately 0.13, and validation loss stabilizes close to 0.25 at epoch 20. The steadily decreasing and closely aligned loss values indicate effective learning and minimal overfitting, reinforcing the model's generalization capability.

Figure 20 shows the accuracy distribution of the suggested model using 5-fold cross-validation, a method for assessing the generalization and durability of the model. With numbers continuously above 96% and reaching a peak of 97% in Fold 3, each bar shows the accuracy attained on one of the five folds. The model's low overfitting and strong generalization skills are demonstrated by the folds' minimum accuracy variation, which sustains performance across several dataset subsets. This demonstrates that the model can identify COVID-19 in actual chest X-ray pictures.

Figure 21 presents a comprehensive analysis of the computational complexity of the proposed method and compares it with other existing methods. The results demonstrate that, with a computational complexity of only 13 ms, the suggested method is more enhanced than the recent models. Specifically, VGG19, VGG16, InceptionV3, Xception, and ResNet50 have processing speeds of 28 ms, 31 ms, 23 ms, and 25.5 ms, respectively. This analysis underscores the efficiency of the suggested approach, which

not only streamlines processing times but also enhances overall performance compared to these well-known architectures. The reduced computational complexity positions the proposed model as a compelling alternative for scenarios where processing speed is critical, demonstrating its suitability for real-time or resource-constrained environments. Consequently, these outcomes demonstrate how effectively the proposed method outperforms popular models such as ResNet50, Xception, InceptionV3, VGG16, and VGG19 while generating faster outcomes.

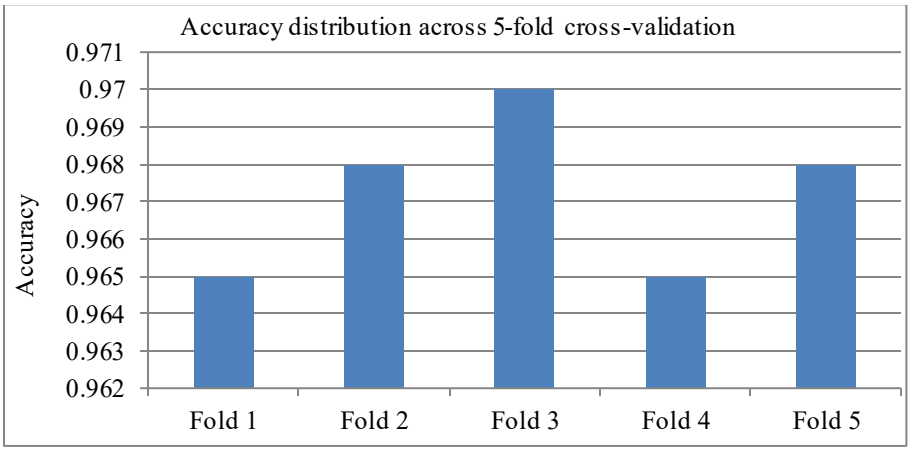

Fig. 20 Accuracy distribution across 5-fold cross-validation

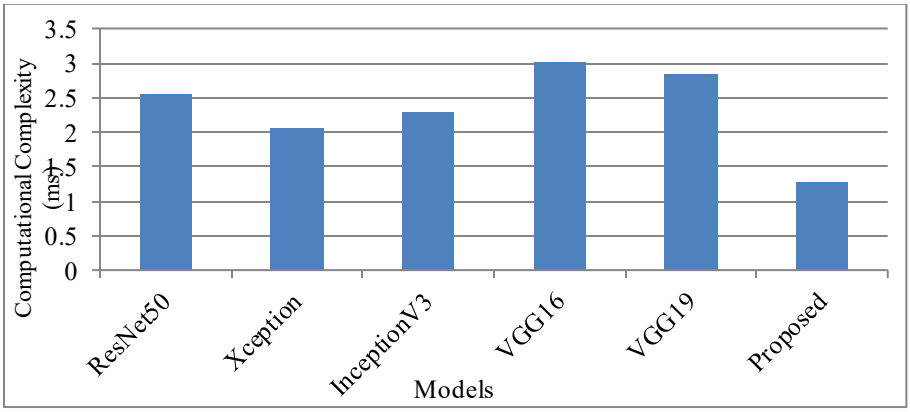

Fig. 21 Computational complexity of the different models

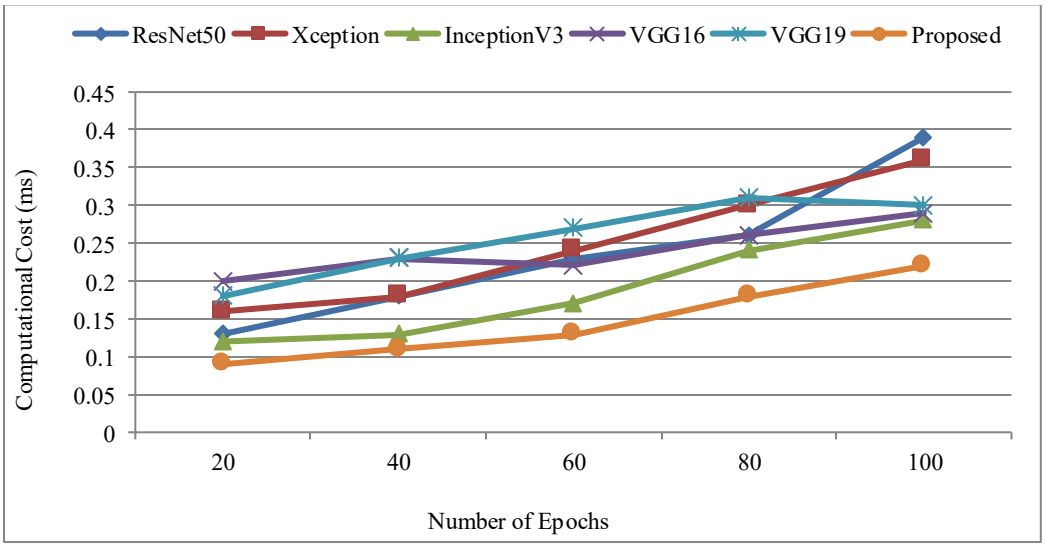

Fig. 22 Computational cost of the different models

The suggested approach and current approaches are compared, and their costs are examined in Figure 22. Lower computing costs indicate the efficiency of the suggested model. The evaluation in this experiment was carried out during a 20-100 epoch period. For the suggested model, the calculation times for 20, 40, 60, 80, and 100 epochs were 0.06 ms, 0.12 ms, 0.135 ms, and 0.22 ms, respectively. On the other hand, the suggested approach showed lower computing costs than the current models. The findings demonstrate that, in comparison to well-established prototypes, the proposed method shows noticeably less computational complexity.

4.6. Discussion

The proposed method aligns with existing literature demonstrating that advanced preprocessing techniques and transfer learning significantly enhance coronavirus detection from CXR images. Specifically, the application of CLAHE improved local contrast, aiding in the detection of subtle opacities, an outcome consistent with findings [40], who reported improved lesion visibility using contrast enhancement. Similarly, the use of Grad-CAM not only validated model decisions but also localized infection regions, reinforcing the explainability of DL models, as supported [41].

EfficientNet-B4's integration offered a fair compromise between computing cost and accuracy, supporting earlier research that emphasizes its scalability and effectiveness in medical imaging. Practically, these findings suggest that combining CLAHE [42], deep transfer learning, and interpretability tools like Grad-CAM can yield reliable, interpretable models for clinical screening, thus supporting radiologists in rapid and accurate coronavirus diagnosis.

4.7. Comparison

A review of existing models in the literature, many have demonstrated strong performance in classifying CXR diseases. For example, the ResNet50 model was 91.78%. Similar research has been done on X-ray images, with Jan et al. classifying three classes: viral, normal, and COVID-19, with an accuracy of 97.20% [43] and Rahhal et al. classifying three classes with an accuracy of 96.79% [24].

In contrast, validation accuracy on a unique dataset using S.Ying et al. obtained 86.00% accuracy [44] while Loey et al. obtained 80.00% accuracy with CT-scan images [45]. In the current study, the maximum validation accuracy reached 97.5% on the augmented dataset when employing the EfficientNet-B4 model.

The suggested approach performed competitively, albeit not outperforming all earlier research in terms of accuracy. Notably, this work provides an improvement over current models by using CT-scan image classification and illness localization in addition to CXR image classification.

4.8. Comparative Analysis with the Literature Papers

The pre-trained Efficient Net B4 models' assessment of the suggested model's classification results is shown in Table 7.

Table 7. Comparing the suggested model's classification performance to CNN models that were previously trained using the COVID-19 radiography database

Author	Year	Model	Dataset	Accuracy	Precision	Recall	F1 score
Ukwuoma et al. [19]	2023	XAI Model	COVID-19 radiography	98%	96%	96%	96%
Nayak, et.al [20]	2023	LW-CBRGPNet	COVID-19 radiography	98.3%	97.8%	98%	98.3%
Hussein, et.al [21]	2022	HQ-CNN model	COVID-19 radiography	98.2%	98.7%	97.9%	99%
Meem, et, al [22]	2022	CNN model	COVID-19 radiography	98.3%	98%	-	97.9%
Ukwuoma et al. [23]	2022	DenseNet201	COVID-19 radiography	96%	92%	-	91%
Rahhal et al. [24]	2022	VGG16	COVID-19 radiography	95.64%	-	-	-
Albahli, et.al [25]	2023	VGG16	COVID-19 radiography	97.3	97%	-	-
Srinivas, et.al [26]	2024	IV3-VGG model	COVID-19 radiography	98%	-	97.8%	98%
Umer, et.al [27]	2022	VGG-16, AlexNet	COVID-19 radiography	98%	97%	98%	-
Proposed		TCov- Efficient net-B4	COVID-19 radiography	98.5%	95%	96%	94%

Table 7 compares the performance metrics of various DL models used for diagnostic categorization on the COVID-19 radiography dataset. The proposed model, TCov-EfficientNet-B4, performs better than the previous tests, achieving the greatest accuracy of 98.5% overall, a competitive F1-score of 94%, and strong precision and recall of 95% and 96%, respectively. While Nayak et al.'s LW-CBRGPNet obtained the greatest F1-score (98.3%) and a somewhat higher accuracy of 98.3%, Ukwuoma et al. (2023) presented an XAI-based model with balanced metrics (98% accuracy, 96% for both precision and recall).

The reliability of Hussein et al.'s HQ-CNN was demonstrated by its remarkable F1 score (99%) and good precision (98.7%). Although some performance metrics were not disclosed, Meem et al. and Umer et al. similarly reported high accuracy (98.3% and 98%, respectively). With accuracies ranging from 95.64% to 98%, conventional architectures such as DenseNet201, VGG16, and hybrid models (IV3-VGG) also showed strong performance. The suggested TCov-EfficientNet-B4 model provides a reliable and accurate method for detecting the coronavirus from radiography pictures, outperforming the majority of current models overall.

5. Conclusion

In conclusion, the medical community is quite concerned about the COVID-19 pandemic's capacity to infect even healthy people. Medical professionals have widely used expert systems to assist them in making early assessments and predictions to stop the virus from spreading. In terms of recognition accuracy and balance, this study's promising AI-based diagnostic model using EfficientNet performed better than several previous models, achieving up to 98.5% validation accuracy and around 97.6% training accuracy on original datasets. Notwithstanding these positive results, the model still has limitations, such as the potential for overfitting, interpretability problems, and limited generalizability due to dataset limitations. Furthermore, it could be challenging to employ in situations with limited resources due to its high reliance on processing resources. In order to improve the model for real-time and resource-constrained scenarios, future research should concentrate on employing explainable AI techniques, diversifying datasets, and adding multi-modal data (such as test results and patient histories). Addressing these aspects will enhance the model's reliability, scalability, and clinical applicability, making it a more effective tool in pandemic response and broader healthcare applications.

References

[1] Isabel Bergeri et al., "Early Epidemiological Investigations: World Health Organization UNITY Protocols Provide a Standardized and Timely International Investigation Framework during the COVID-19 Pandemic," *Influenza and Other Respiratory Viruses*, vol. 16, no. 1, pp. 7-13, 2022. [CrossRef] [Google Scholar] [Publisher Link]

[2] Awad A. Shehata et al., "Diversity of Coronaviruses with Particular Attention to the Interspecies Transmission of SARS-CoV-2," *Animals*, vol. 12, no. 3, pp. 1-21, 2022. [CrossRef] [Google Scholar] [Publisher Link]

[3] Ke Men et al., "Estimate the Incubation Period of Coronavirus 2019 (COVID-19)," *Computers in Biology and Medicine*, vol. 158, pp. 1-12, 2023. [CrossRef] [Google Scholar] [Publisher Link]

[4] Anacleto Silva de Souza et al., "Severe Acute Respiratory Syndrome Coronavirus 2 Variants of Concern: A Perspective for Emerging More Transmissible and Vaccine-Resistant Strains," *Viruses*, vol. 14, no. 4, pp. 1-21, 2022. [CrossRef] [Google Scholar] [Publisher Link]

[5] Prafull Kamble et al., "Synopsis of Symptoms of COVID-19 during the Second Wave of the Pandemic in India," *Hormone Molecular Biology and Clinical Investigation*, vol. 43, no. 1, pp. 97-104, 2022. [CrossRef] [Google Scholar] [Publisher Link]

[6] Alana Teles Costa et al., "Policy Responses from Countries with the Highest Number of COVID-19 Deaths in the World: A Scoping Review," *Research, Society and Development*, vol. 11, no. 12, pp. 1-15, 2022. [CrossRef] [Google Scholar] [Publisher Link]

[7] Pei-Chin Lin et al., "Diagnostic Performance of GenBody COVID-19 Rapid Antigen Test for Laboratory and Non-Laboratory Medical Professionals in Real Practice: A Retrospective Study," *Medicine*, vol. 102, no. 33, pp. 1-5, 2023. [CrossRef] [Google Scholar] [Publisher Link]

[8] Inayatullah Shah Sayed, and Nor Fitri Toh Man Hua, "Role of X-Ray CT, Plain Radiography and Ultrasound Imaging in Diagnosing COVID-19: A Narrative Review," *International Journal of Allied Health Sciences*, vol. 7, no. 2, pp. 2933-2944, 2023. [Google Scholar] [Publisher Link]

[9] Shahanaz Abdul Gafoor et al., "Deep Learning Model for Detection of COVID-19 Utilizing the Chest X-Ray Images," *Cogent Engineering*, vol. 9, no. 1, pp. 1-18, 2022. [CrossRef] [Google Scholar] [Publisher Link]

[10] Claudia Ravaglia et al., "Clinical, Radiological and Pathological Findings in Patients with Persistent Lung Disease Following SARS-CoV-2 Infection," *European Respiratory Journal*, vol. 60, no. 4, pp. 1-11, 2022. [CrossRef] [Google Scholar] [Publisher Link]

[11] Sajid Iqbal et al., *COVID-19 Prediction, Diagnosis and Prevention through Computer Vision*, Prognostic Models in Healthcare: AI and Statistical Approaches, Springer, Singapore, pp. 79-113, 2022. [CrossRef] [Google Scholar] [Publisher Link]

[12] Kirti Raj Bhatele et al., "COVID-19 Detection: A Systematic Review of Machine and Deep Learning-Based Approaches Utilizing Chest X-Rays and CT Scans," *Cognitive Computation*, vol. 16, no. 4, pp. 1889-1926, 2024. [CrossRef] [Google Scholar] [Publisher Link]

[13] Luca Brunese et al., "Explainable Deep Learning for Pulmonary Disease and Coronavirus COVID-19 Detection from X-Rays," *Computer Methods and Programs in Biomedicine*, vol. 196, pp. 1-11, 2020. [CrossRef] [Google Scholar] [Publisher Link]

[14] Mamta Patel, and Mehul Shah, "Transfer Learning with Fine-Tuned Deep CNN Model for COVID-19 Diagnosis from Chest X-ray Images," *International Journal of Advanced Technology and Engineering Exploration*, vol. 10, no. 103, pp. 1-21, 2023. [CrossRef] [Google Scholar] [Publisher Link]

[15] Saeed Iqbal et al., "Dynamic Learning for Imbalanced Data in Learning Chest X-Ray and CT Images," *Heliyon*, vol. 9, no. 6, pp. 1-20, 2023. [CrossRef] [Google Scholar] [Publisher Link]

[16] Morsheda Akter et al., "Human Activity Recognition using Attention-Mechanism-based Deep Learning Feature Combination," *Sensors*, vol. 23, no. 12, pp. 1-15, 2023. [CrossRef] [Google Scholar] [Publisher Link]

[17] Farhad Maleki et al., "Generalizability of Machine Learning Models: Quantitative Evaluation of Three Methodological Pitfalls," *Radiology: Artificial Intelligence*, vol. 5, no. 1, pp. 1-10, 2022. [CrossRef] [Google Scholar] [Publisher Link]

[18] Chiagoziem C. Ukwuoma et al., "Multi-Classification of Breast Cancer Lesions in Histopathological Images using DEEP_Pachi: Multiple Self-Attention Head," *Diagnostics*, vol. 12, no. 5, pp. 1-32, 2022. [CrossRef] [Google Scholar] [Publisher Link]

[19] Chiagoziem C. Ukwuoma et al., "Deep Learning Framework for Rapid and Accurate Respiratory COVID-19 Prediction using Chest X-ray Images," *Journal of King Saud University - Computer and Information Sciences*, vol. 35, no. 7, pp. 1-16, 2023. [CrossRef] [Google Scholar] [Publisher Link]

[20] Soumya Ranjan Nayak et al., "An Automated Lightweight Deep Neural Network for Diagnosis of COVID-19 from Chest X-ray Images," *Arabian Journal for Science and Engineering*, vol. 48, no. 8, pp. 11085-11102, 2023. [CrossRef] [Google Scholar] [Publisher Link]

[21] Essam H Houssein et al., "Hybrid Quantum-Classical Convolutional Neural Network Model for COVID-19 Prediction using Chest X-ray Images," *Journal of Computational Design and Engineering*, vol. 9, no. 2, pp. 343-363, 2022. [CrossRef] [Google Scholar] [Publisher Link]

[22] Anika Tahsin Meem et al., "Prediction of COVID-19 based on Chest X-ray Images using Deep Learning with CNN," *Computer Systems Science and Engineering*, vol. 41, no. 3, pp. 1223-1240, 2022. [CrossRef] [Google Scholar] [Publisher Link]

[23] Chiagoziem C. Ukwuoma et al., "Automated Lung-Related Pneumonia and COVID-19 Detection based on Novel Feature Extraction Framework and Vision Transformer Approaches using Chest X-ray Images," *Bioengineering*, vol. 9, no. 11, pp. 1-27, 2022. [CrossRef] [Google Scholar] [Publisher Link]

[24] Mohamad Mahmoud Al Rahhal et al., "Contrasting EfficientNet, ViT, and gMLP for COVID-19 Detection in Ultrasound Imagery," *Journal of Personalized Medicine*, vol. 12, no. 10, pp. 1-17, 2022. [CrossRef] [Google Scholar] [Publisher Link]

[25] Saleh Albahli, and Ghulam Nabi Ahmad Hassan Yar, "Efficient Grad-Cam-Based Model for COVID-19 Classification and Detection," *Computer Systems Science and Engineering*, vol. 44, no. 3, pp. 2743-2757, 2023. [CrossRef] [Google Scholar] [Publisher Link]

[26] K. Srinivas et al., "COVID-19 Prediction based on Hybrid Inception V3 with VGG16 using Chest X-ray Images," *Multimedia Tools and Applications*, vol. 83, no. 12, pp. 36665-36682, 2024. [CrossRef] [Google Scholar] [Publisher Link]

[27] Muhammad Umer et al., "COVINet: A Convolutional Neural Network Approach for Predicting COVID-19 from Chest X-Ray Images," *Journal of Ambient Intelligence and Humanized Computing*, vol. 13, no. 1, pp. 535-547, 2022. [CrossRef] [Google Scholar] [Publisher Link]

[28] Md. Nahiduzzaman, Md. Rabiul Islam, and Rakibul Hassan, "ChestX-Ray6: Prediction of Multiple Diseases Including COVID-19 from Chest X-ray Images using Convolutional Neural Network," *Expert Systems with Applications*, vol. 211, pp. 1-14, 2023. [CrossRef] [Google Scholar] [Publisher Link]

[29] Mohit Kumar et al., "COVID-19 Prediction through X-Ray Images using Transfer Learning-based Hybrid Deep Learning Approach," *Materials Today: Proceedings*, vol. 51, pp. 2520-2524, 2022. [CrossRef] [Google Scholar] [Publisher Link]

[30] A. Arivoli, Devdatt Golwala, and Rayirth Reddy, "CoviExpert: COVID-19 Detection from Chest X-Ray using CNN," *Measurement: Sensors*, vol. 23, pp. 1-8, 2022. [CrossRef] [Google Scholar] [Publisher Link]

[31] Kaiming He et al., "Deep Residual Learning for Image Recognition," *2016 IEEE Conference on Computer Vision and Pattern Recognition (CVPR)*, Las Vegas, NV, USA, pp. 770-778, 2016. [CrossRef] [Google Scholar] [Publisher Link]

[32] Karen Simonyan, and Andrew Zisserman, "Very Deep Convolutional Networks for Large-Scale Image Recognition," *3rd International Conference for Learning Representations*, San Diego, CA, USA, pp. 1-14, 2015. [Google Scholar] [Publisher Link]

[33] François Chollet, "Xception: Deep Learning with Depth-Wise Separable Convolutions," *2017 IEEE Conference on Computer Vision and Pattern Recognition (CVPR)*, Honolulu, HI, USA, pp. 1800-1807, 2017. [CrossRef] [Google Scholar] [Publisher Link]

[34] Saleh Albahli, Nasir Ayub, and Muhammad Shiraz, "Coronavirus Disease (COVID-19) Detection using X-ray Images and Enhanced DenseNet," *Applied Soft Computing*, vol. 110, pp. 1-10, 2021. [CrossRef] [Google Scholar] [Publisher Link]

[35] Tawsifur Rahman, Muhammad Chowdhury, and Amith Khandakar, COVID-19 Radiography Database, Kaggle, 2020. [Online]. Available: https://www.kaggle.com/tawsifurrahman/COVID19-radiography-database

[36] Amal H. Alharbi et al., "Detection of Peripheral Malarial Parasites in Blood Smears using Deep Learning Models," *Computational Intelligence and Neuroscience*, vol. 2022, pp. 1-11, 2022. [CrossRef] [Google Scholar] [Publisher Link]

[37] Xuebin Yue et al., "Machine Learning-based Apathy Classification on Doppler Radar Image for the Elderly Person," *Procedia Computer Science*, vol. 187, pp. 146-151, 2021. [CrossRef] [Google Scholar] [Publisher Link]

[38] Naoto Nojiri et al., "Apathy Classification based on Doppler Radar Image for the Elderly Person," *Frontiers in Bioengineering and Biotechnology*, vol. 8, pp. 1-16, 2020. [CrossRef] [Google Scholar] [Publisher Link]

[39] Lin Meng et al., "Oracle Bone Inscription Detector based on SSD," *International Conference on Image Analysis and Processing, Trento, Italy*, pp. 126-136, 2019. [CrossRef] [Google Scholar] [Publisher Link]

[40] Asmaa Abbas, Mohammed M. Abdelsamea, and Mohamed Medhat Gaber, "Classification of COVID-19 in Chest X-Ray Images using DeTraC Deep Convolutional Neural Network," *Applied Intelligence*, vol. 51, no. 2, pp. 854-864, 2021. [CrossRef] [Google Scholar] [Publisher Link]

[41] Ramprasaath R. Selvarajuet al., "Grad-CAM: Visual Explanations from Deep Networks via Gradient-Based Localization," *International Journal of Computer Vision*, vol. 128, no. 2, pp. 336-359, 2020. [CrossRef] [Google Scholar] [Publisher Link]

[42] Mingxing Tan, and Quoc Le, "EfficientNet: Rethinking Model Scaling for Convolutional Neural Networks," *Proceedings of the 36th International Conference on Machine Learning*, Long Beach, California, vol. 97, pp. 6105-6114, 2019. [Google Scholar] [Publisher Link]

[43] Chia-Wei Jan et al., "Optical based Gradient-Weighted Class Activation Mapping and Transfer Learning Integrated Pneumonia Prediction Model," *Computer Systems Science and Engineering*, vol. 47, no. 3, pp. 2989-3010, 2023. [CrossRef] [Google Scholar] [Publisher Link]

[44] Ying Song et al., "Deep Learning Enables Accurate Diagnosis of Novel Coronavirus (COVID-19) with CT Images," *IEEE/ACM Transactions on Computational Biology and Bioinformatics*, vol. 18, no. 6, pp. 2775-2780, 2021. [CrossRef] [Google Scholar] [Publisher Link]

[45] Mohamed Loey, Florentin Smarandache, and Nour Eldeen M. Khalifa, "Within the Lack of Chest COVID-19 X-Ray Dataset: A Novel Detection Model based on GAN and Deep Transfer Learning," *Symmetry*, vol. 12, no. 4, pp. 1-19, 2020. [CrossRef] [Google Scholar] [Publisher Link]